Nanoscale

ROYAL SOCIETY
OF **CHEMISTRY**

PAPER
Jae-Hyung Jang *et al.*
Luminescent down-shifting CsPbBr$_3$ perovskite nanocrystals
for flexible Cu(In,Ga)Se$_2$ solar cells

NCNST

Nanoscale

PAPER

Check for updates

Luminescent down-shifting CsPbBr₃ perovskite nanocrystals for flexible Cu(In,Ga)Se₂ solar cells†

Ye-Chan Kim,[a] Ho-Jung Jeong,[b] Sung-Tae Kim,[a] Young Hyun Song,[b] Bo Young Kim,[b] Jae Pil Kim,[b] Bong Kyun Kang,[c] Ju-Hyung Yun [ID][d] and Jae-Hyung Jang [ID] *[a]

To overcome the parasitic absorption of ultraviolet (UV) light in the transparent conductive oxide (TCO) layer of flexible Cu(In,Ga)Se₂ (CIGS) thin film solar cells, a CsPbBr₃ perovskite nanocrystal based luminescent down-shifting (LDS) layer was integrated on CIGS solar cells fabricated on a stainless steel foil. The CsPbBr₃ perovskite nanocrystal absorbs solar irradiation at wavelengths shorter than 520 nm and emits photons at a wavelength of 532 nm. These down-shifted photons pass the TCO layer without parasitic absorption and are absorbed in the CIGS absorber layer where they generate photocurrent. By minimizing the parasitic absorption in the TCO layer, the external quantum efficiency (EQE) of the CIGS solar cell with the CsPbBr₃ perovskite nanocrystal layer is highly improved in the UV wavelength range between 300 and 390 nm. Additionally, in the wavelength range between 500 and 1100 nm, the EQE is improved since the surface reflectance of the CIGS device with the CsPbBr₃ perovskite LDS layer was reduced. This is because the CsPbBr₃ perovskite nanocrystal layer, which has an effective refractive index of 1.82 at a wavelength of 800 nm, reduces the large refractive index mismatch between air (n_{air} = 1.00) and the TCO layer (n_{ZnO} = 1.96 at a wavelength of 800 nm). Both the short circuit current density and power conversion efficiency of the flexible CIGS solar cell integrated with the CsPbBr₃ perovskite are improved by 4.5% compared with the conventional CIGS solar cell without the CsPbBr₃ perovskite LDS layer.

Introduction

The photovoltaic performance of thin film solar cells based on Cu(In,Ga)Se₂ (CIGS), Cu₂ZnSnS₄ and CdTe has mainly been improved by advances in material synthesis techniques[1–4] and device structures, including the buffer and window layer.[5–8] However, these thin film solar cells have suffered from optical losses due to surface reflection, the shading effect of the metal grid and ultraviolet (UV) light absorption in the transparent conductive oxide (TCO) layer. These factors limit further improvements in the photovoltaic performance of the devices. The surface reflection and shading effects have been effectively addressed by using micro or nano-engineered structures.[9–11] However, the UV light absorption problem remains unresolved. Generally, ZnO related materials and Sn doped In₂O₃ (ITO) have been used as the TCO layer of thin film solar cells. To overcome the UV absorption in the TCO layer, wide band gap materials, such as MoO$_x$,[12] In₂O₃[13] and Cd₂SnO₄,[14] were investigated but they were inefficient at improving the photovoltaic performance, due to their higher resistivity compared to ZnO related materials and ITO.

Another approach to prevent UV light absorption in the TCO layer is to integrate luminescent down-shifting (LDS) materials on top of the solar cells.[15,16] The schematic designs of the conventional CIGS solar cells and the ones integrated with the LDS layer are shown in Fig. 1(a) and (b), respectively. The LDS layer absorbs high energy photons and emits lower energy photons which pass through the TCO layer and reach the CIGS absorption layer. The low energy photons are absorbed in the absorber layer and contribute to photocurrent generation.[15] Quantum dots based on Cd or Cu, organic dyes, and rare earth elements have been investigated for LDS materials.[15,17] However, these LDS materials have drawbacks, such as the high material cost and complex fabrication process. Low cost LDS material synthesis processes and a simple integration process still require investigation.

[a]School of Electrical Engineering and Computer Science, Gwangju Institute of Science and Technology (GIST), Cheomdangwagi-ro, Buk-gu, Gwangju, 61005, Republic of Korea. E-mail: yckim@gist.ac.kr
[b]Lighting Materials and Components Research Center, Korea Photonics Technology Institute (KOPTI), Gwangju 61007, Republic of Korea. E-mail: hojung@kopti.re.kr
[c]Nano Materials and Components Research Center, Korea Electronics Technology Institute, Seongnam 463-816, Republic of Korea
[d]Department of Electrical Engineering, Incheon National University, Yeonsu-gu, Incheon 406-772, Republic of Korea
†Electronic supplementary information (ESI) available. See DOI: 10.1039/c9nr06041c
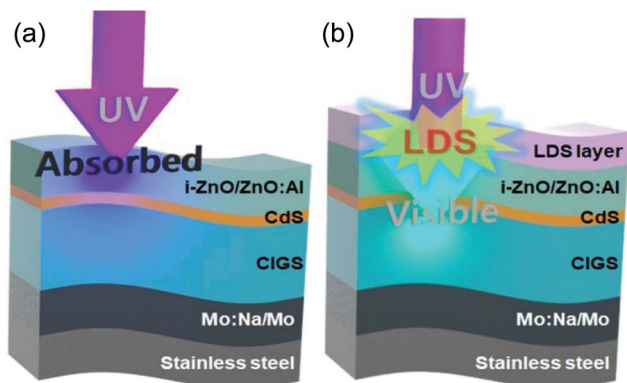
Fig. 1 The schematic design of the conventional (a) and LDS layer integrated (b) CIGS solar cell.

The $CsPbX_3$ (X = Cl, Br, I) perovskite nanocrystal is one of the candidates for low cost LDS materials because it is easy to synthesize using a solution process. It also provides a couple of advantages, such as tunability of the emission wavelength from the visible to the infrared region by controlling its composition,[18,19] and narrow band emission characteristics that prevent the re-absorption loss of the emitted photons.[20,21] Given these excellent optical properties, $CsPbX_3$ perovskite nanocrystals deserve to be applied as the LDS layer. Recently, Donglei Zhou *et al.* achieved highly improved power conversion efficiency (PCE) by integrating a $CsPbBr_3$ perovskite based LDS layer on a Si solar cell.[22] However, it required rare earth dopants such as Ce and Yb. It is also difficult to use in CIGS solar cells because its emissions, centered at 450 nm, are absorbed in the CdS buffer layer.

In this work, pure $CsPbBr_3$ perovskite nanocrystals were integrated as the LDS layer on flexible CIGS solar cells to overcome the parasitic absorption of UV light in the TCO layer. The structural and optical characteristics of the $CsPbBr_3$ perovskite nanocrystals were analysed and the device performances of the CIGS solar cell with and without the $CsPbBr_3$ perovskite LDS layer were compared, to study the effect of the $CsPbBr_3$ perovskite LDS layer.

Experiments

To prepare the 0.1 M Cs-oleate solution, Cs_2CO_3 (0.8 g), 1-octadecene (ODE, 30 mL) and oleic acid (OA, 2.5 mL) were loaded into a 50 mL three neck flask and then stirred for 1 hour at 120 °C under vacuum. Subsequent heating at 150 °C under nitrogen purge for 10 minutes resulted in a clear 0.1 M Cs-oleate solution. The obtained solution was cooled to 100 °C before injection. Meanwhile, a precursor solution was prepared by adding $PbBr_2$ (0.138 g) and ODE (10 mL) into a 50 mL three neck flask and then heated at 120 °C for 1 hour under vacuum. OA (1 mL) and oleylamine (1 mL) were added into the precursor solution and the temperature was raised to 180 °C. When the temperature of the precursor solution reached

180 °C, the prepared Cs-oleate solution (100 °C, 0.8 mL) was quickly injected. Crystallization begins immediately. After crystallization for 5 seconds, the $CsPbBr_3$ perovskite nanocrystals were cooled to room temperature by transferring them into an ice water bath to stop further crystallization. To collect pure $CsPbBr_3$ perovskite nanocrystals, the products were centrifuged at 5000 rpm for 10 min and then precipitates were dispersed in 5 mL toluene. This centrifugation process was repeated three times to eliminate the non-reacting agent. The final precipitates were re-dispersed in 2 mL of toluene.

The flexible CIGS solar cells were fabricated on top of 100 μm thick stainless steel (STS) substrates. A 300 nm thick Na-doped Mo (Mo:Na) and 1 μm thick Mo were deposited by dc sputtering in sequence. The CIGS absorber layer was grown on Mo:Na/Mo coated STS by the three stage co-evaporation process.[4] Details of the CIGS growth and device fabrication processes are reported elsewhere.[15] As shown in Fig. 1(a), the completed CIGS device has a Al–Ni metal grid/ZnO:Al–ZnO window layer/CdS buffer layer/CIGS absorber layer/Mo based back contact/STS substrate (1.0/0.4/0.06/2.0/1.3/100 μm) structure.

To investigate the effects of the $CsPbBr_3$ based LDS layer on the photovoltaic performance of the devices, a 730 nm thick $CsPbBr_3$ perovskite LDS layer was deposited on top of the CIGS devices by spin coating at 2000 rpm for 30 seconds. Afterwards, to evaporate the remaining toluene solvent, the coated samples were annealed at 80 °C for 10 min on a hot plate.

The morphology and crystallinity of the $CsPbBr_3$ perovskite nanocrystals were characterized using scanning electron microscopy (SEM, S-4700, Hitachi) and transmission electron microscopy (TEM, JEM-2100F, JEOL) with an accelerating voltage of 200 kV. The absorbance and photoluminescence (PL) were investigated by using a UV-VIS-IR spectrophotometer (Cary-5000, Varian) and PL spectroscope (RPM 2000, ACCENT) equipped with a He–Cd laser (325 nm), respectively. The external quantum efficiency (EQE) of the solar cells was measured with an incident photon to electron conversion efficiency measurement system (QEX7, PV measurement) calibrated by certified reference Si and Ge photodiodes. The current density–voltage (J–V) characteristics of the CIGS solar cells were measured with an Air Mass 1.5G solar simulator (Oriel Sol3A Class AAA, Newport) with an irradiation intensity of 100 W m^{-2}.

Results and discussion

The morphology and crystallinity of the synthesized $CsPbBr_3$ perovskite nanocrystals were analyzed by SEM and TEM. A cross sectional SEM image of the 730 nm thick $CsPbBr_3$ perovskite on the CIGS device is shown in Fig. 2(a). The heterointerfaces and the thickness of each material are clearly observed. The plane view SEM image in Fig. 2(b) shows that the surface of the CIGS device is fully covered by uniformly distributed $CsPbBr_3$ perovskite nanocrystals. A TEM image of the
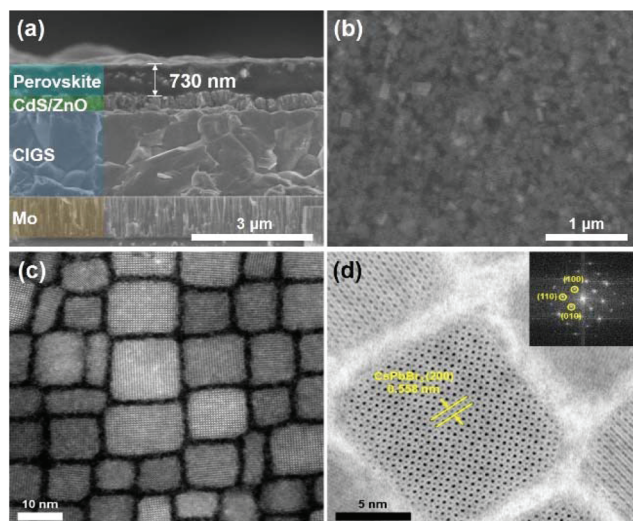
Fig. 2 (a) Cross sectional and (b) plane view SEM images of the $CsPbBr_3$ perovskite on the CIGS device. (c) TEM and (d) HR-TEM images of the $CsPbBr_3$ perovskite nanocrystals. The inset shows the diffraction pattern of the $CsPbBr_3$ perovskite nanocrystals.

$CsPbBr_3$ perovskite nanocrystals is shown in Fig. 2(c). Cubic shaped $CsPbBr_3$ perovskite nanocrystals, whose diagonal length is in the range of 8–18 nm, are observed. Fig. 2(d) shows a high resolution (HR)-TEM image and the diffraction pattern as an inset. Highly crystallized $CsPbBr_3$ perovskite nanocrystals and a lattice spacing of 0.558 nm corresponding to the (100) lattice plane are observed. In the XRD pattern, the three strong peaks of (101), (121), and (202) are observed at 15.14°, 21.40°, and 30.70°, respectively (ESI Fig. S1†). It implies that the $CsPbBr_3$ perovskite nanocrystals are highly crystallized because the XRD pattern is well matched with JCPDS 18-0364.

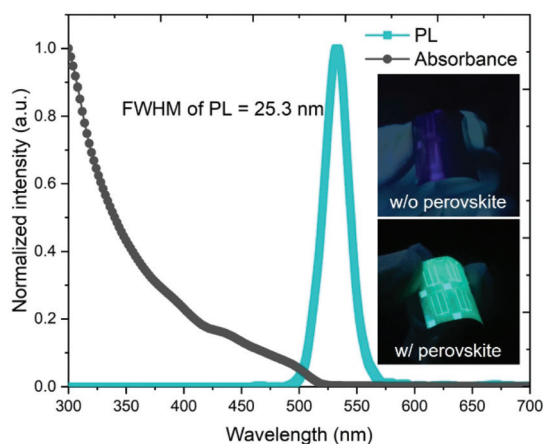The absorbance and PL spectra are shown in Fig. 3. The $CsPbBr_3$ perovskite nanocrystals absorb UV light ranging from

300 to 520 nm and emit photons with a wavelength of 532 nm. The emitted photons are transmitted to the CIGS absorber layer and generate photocurrent. The measured full width at half maximum (FWHM) of 25.3 nm in the emission spectrum is much narrower than those of the other LDS materials.[23] Furthermore, the transmittance is greater than 90% in the wavelength range between 520 and 1200 nm (Fig. S2†). However, it decreases abruptly at wavelengths shorter than 520 nm due to light absorption by the $CsPbBr_3$ perovskite. Photographs taken under UV light with a wavelength of 325 nm are shown in the inset of Fig. 3. Under UV illumination, a green light emission is observed in the CIGS solar cell integrated with the $CsPbBr_3$ perovskite, whereas there is no PL on the conventional CIGS solar cell without the perovskite.

To analyse the spectral response, the EQEs of the CIGS devices with and without $CsPbBr_3$ perovskites were characterized, as shown in Fig. 4(a). While the EQE of the conventional CIGS solar cell is nearly zero in the wavelength range between 300 and 340 nm, due to parasitic UV light absorption in the TCO layer, the EQE of the CIGS solar cell integrated with the $CsPbBr_3$ perovskite is highly improved in the wavelength range between 300 and 390 nm (Region 1). It is because the $CsPbBr_3$
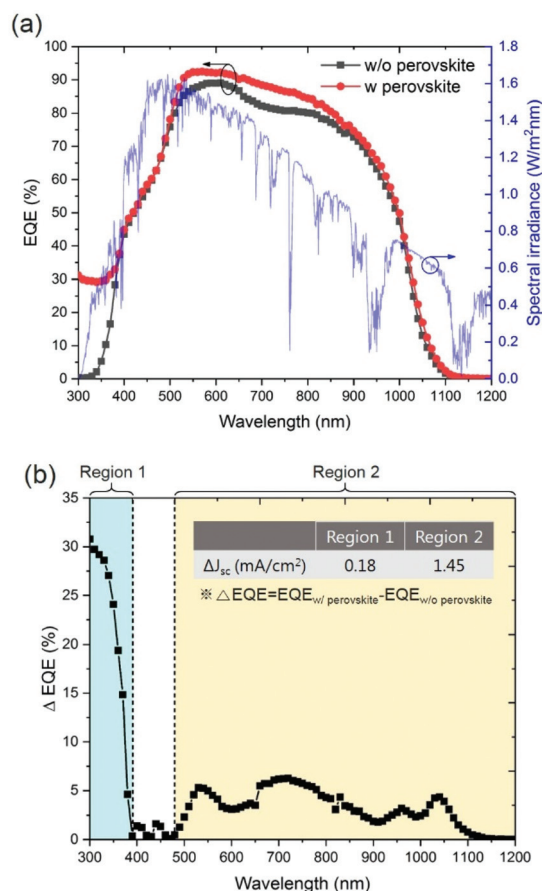

Fig. 3 The PL and absorbance spectra of the $CsPbBr_3$ perovskite nanocrystals. The inset shows photographs of the CIGS devices with and without the $CsPbBr_3$ perovskite LDS layer taken under UV light with a wavelength of 325 nm.

Fig. 4 (a) EQE graphs of the flexible CIGS solar cell with and without $CsPbBr_3$ perovskite nanocrystals. (b) ΔEQE spectrum. The inset shows the ΔJ_{sc} calculated from eqn (1) in regions 1 and 2.

perovskite based LDS layer absorbs short wavelength light between 300 and 520 nm and emits visible light with a wavelength of 532 nm. The energy down-converted photons reach the CIGS absorber layer without parasitic absorption in the TCO layer.

In addition, the improved EQE is observed for the CIGS solar cell with the CsPbBr$_3$ perovskite in the wavelength range between 500 and 1100 nm (Region 2), indicating that the LDS layer acts as an anti-reflection coating (ARC) as well. The large refractive index mismatch between the air (n_{air} = 1.00) and TCO layer (n_{ZnO} = 1.96 at 800 nm wavelength) was reduced by the CsPbBr$_3$ perovskite layer which has an effective refractive index of 1.82 at a wavelength of 800 nm (Fig. S3†). The surface reflectance of the CIGS device with a CsPbBr$_3$ perovskite LDS layer is much lower than that of the CIGS solar cell without a LDS layer (Fig. S4†)

As shown in Fig. 4(b), the improvement in EQE (ΔEQE) distinctively observed in regions 1 and 2 results from the effects of LDS and ARC, respectively. The current density gain (ΔJ_{sc}) calculated from the EQE between λ_1 and λ_2 can be expressed as

$$\Delta J_{sc} = \int_{\lambda_1}^{\lambda_2} q \times \Phi_{AM1.5G}(\lambda) \times \Delta EQE(\lambda) d\lambda, \qquad (1)$$

where λ is the wavelength, q is the charge of the electron, and $\Phi_{AM1.5G}(\lambda)$ is the photon flux of the AM1.5G solar spectrum. As shown in the inset of Fig. 4(b), the ΔJ_{sc} values calculated from eqn (1) are 0.18 and 1.45 mA cm^{-2} in regions 1 and 2, respectively.

The J–V characteristics were measured by using a solar simulator under an irradiation intensity of 100 W m^{-2}. The J–V characteristics of the CIGS solar cells with and without the CsPbBr$_3$ perovskite are shown in Fig. 5, and the photovoltaic performance parameters of the two types of solar cells are shown in the inset of Fig. 5. The open circuit voltage (V_{oc}) and the fill factor are invariant, whereas both short circuit current density (J_{sc}) and PCE of the CIGS solar cell with the CsPbBr$_3$

perovskite are improved by 4.5% compared with those of the conventional CIGS solar cell without the CsPbBr$_3$ perovskite LDS layer. The flexible CIGS solar cell integrated with the CsPbBr$_3$ perovskite LDS layer exhibits a J_{sc} of 37.2 mA cm^{-2}, V_{oc} of 0.56 V, fill factor of 56.2% and PCE of 11.6%.

Conclusions

An LDS layer based on CsPbBr$_3$ perovskite nanocrystals was integrated on flexible Cu(In,Ga)Se$_2$ (CIGS) thin film solar cells to overcome the parasitic UV light absorption loss in the TCO layer. The EQE is highly improved by the CsPbBr$_3$ perovskite based LDS layer in the UV range between 300 and 390 nm. The LDS layer absorbs solar irradiation at wavelengths shorter than 520 nm and emits photons at a wavelength of 532 nm. These emitted photons are harvested in the CIGS absorber layer without parasitic absorption loss in the TCO layer. Additionally, the AR properties of the CsPbBr$_3$ perovskite are observed in the wavelength range between 500 and 1100 nm. As a result, the J_{sc} and PCE of the CIGS solar cell with the CsPbBr$_3$ perovskite are improved by 4.5% compared with those of the conventional CIGS solar cell without the CsPbBr$_3$ perovskite LDS layer.

Author contributions

The manuscript was written through contributions from all of the authors. All of the authors gave their approval to the final version of the manuscript. Ye-Chan Kim and Ho-Jung Jeong contributed equally to this work and should be considered as co-first authors.

Conflicts of interest

There are no conflicts to declare.

Acknowledgements

Fig. 5 *J*–*V* characteristics of the CIGS solar cells with and without the CsPbBr$_3$ perovskite. The inset table compares photovoltaic performance parameters of the two types of solar cells.

Notes and references

1 A. Chirilă, P. Reinhard, F. Pianezzi, P. Bloesch, A. R. Uhl, C. Fella, L. Kranz, D. Keller, C. Gretener, H. Hagendorfer,
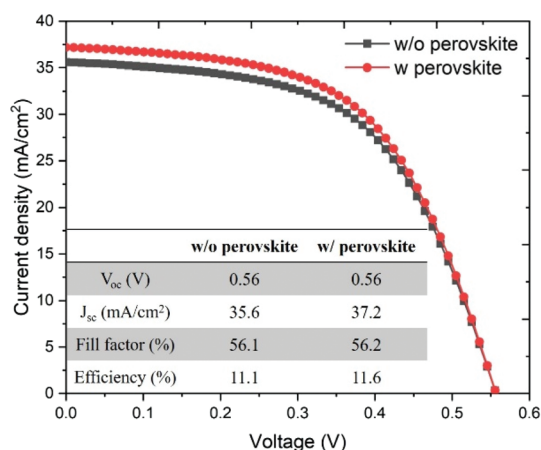
D. Jaeger, R. Erni, S. Nishiwaki, S. Buecheler and A. N. Tiwari, *Nat. Mater.*, 2013, **12**, 1107–1111.

2 W. Wang, M. T. Winkler, O. Gunawan, T. Gokmen, T. K. Todorov, Y. Zhu and D. B. Mitzi, *Adv. Energy Mater.*, 2014, **4**, 1301465.

3 M. Gloeckler, I. Sankin and Z. Zhao, *IEEE J. Photovoltaics*, 2013, **3**, 1389–1393.

4 M. A. Contreras, J. Tuttle, A. Gabor, A. Tennant, K. Ramanathan, S. Asher, A. Franz, J. Keane, L. Wang, J. Scofield and R. Noufi, Conference Record of the 24th IEEE Photovoltaics Specialists Conference, 1994, pp. 68–75.

5 L. M. Mansfield, R. L. Garris, K. D. Counts, J. R. Sites, C. P. Thompson, W. N. Shafarman and K. Ramanathan, *IEEE J. Photovoltaics*, 2017, **7**, 286–293.

6 T. Nakada, Y. Hirabayashi, T. Tokado, D. Ohmori and T. Mise, *Sol. Energy*, 2004, **77**, 739–747.

7 T. Nakada and M. Mizutani, *Jpn. J. Appl. Phys.*, 2002, **41**, 165–167.

8 T. Minemoto, Y. Hashimoto, T. Satoh, T. Negami and H. Takakura, *J. Appl. Phys.*, 2001, **89**, 8327–8330.

9 S. K. Lee, H. J. Jeong, Y. C. Kim and J. H. Jang, *Sol. Energy Mater. Sol. Cells*, 2018, **186**, 254–258.

10 Y. M. Song, Y. Jeong, C. Il Yeo and Y. T. Lee, *Opt. Express*, 2012, **20**, A916–A923.

11 D. S. Kim, S. H. Eo and J. H. Jang, *J. Vac. Sci. Technol., B.*, 2013, **31**(3), 031202.

12 S. I. Park, J. S. Im, L. Fang, J. W. Jeon and K. S. Lim, *Appl. Phys. Lett.*, 2015, **99**, 063504.

13 J. Keller, J. Lindahl, M. Edoff, L. Stolt and T. Törndahl, *Prog. Photovolt: Res. Appl.*, 2016, **24**, 102–107.

14 X. Wu, P. Sheldon, T. J. Coutts, D. H. Rose, W. P. Mulligan and H. R. Moutinho, *AIP Conf. Proc.*, 1997, **394**, 693–702.

15 H. J. Jeong, Y. C. Kim, S. K. Lee, Y. Jeong, J. W. Song, J. H. Yun and J. H. Jang, *ACS Appl. Mater. Interfaces*, 2017, **9**, 25404–25411.

16 H. Chen, C. Lin, H. Han, Y. Tsai, C. Chang, H. Wang, M. Tsai, H. Kuo and P. Yu, *Opt. Express*, 2011, **19**, A1141–A1147.

17 M. Alexandre, M. Chapa, S. Haque, M. J. Mendes, A. Hugo, E. Fortunato and R. Martins, *Adv. Energy Mater.*, 2019, **2**(4), 2930–2938.

18 Y. Wang, X. Li, J. Song, L. Xiao, H. Zeng and H. Sun, *Adv. Mater.*, 2015, **27**, 7101–7108.

19 Y. H. Song, J. S. Yoo, B. K. Kang, S. H. Choi, E. K. Ji, H. S. Jung and D. H. Yoon, *Nanoscale*, 2016, **8**, 19523–19526.

20 W. Zhang, G. E. Eperon and H. J. Snaith, *Nat. Energy*, 2016, **1**, 16048.

21 B. R. Sutherland and E. H. Sargent, *Nat. Photonics*, 2016, **10**, 295–302.

22 D. Zhou, D. Liu, G. Pan, X. Chen, D. Li, W. Xu, X. Bai and H. Song, *Adv. Mater.*, 2017, **29**, 1704149.

23 U. Resch-genger, M. Grabolle, S. Cavaliere-jaricot, R. Nitschke and T. Nann, *Nat. Methods*, 2008, **5**, 763–775.